Time-resolved study of amplitude modulation effects in surface-wave atmospheric pressure argon plasma jet

2014 J. Phys. D: Appl. Phys. 47 085204

(http://iopscience.iop.org/0022-3727/47/8/085204)

IOP Publishing Journal of Physics D: Applied Physics

J. Phys. D: Appl. Phys. **47** (2014) 085204 (11pp) doi:10.1088/0022-3727/47/8/085204

Time-resolved study of amplitude modulation effects in surface-wave atmospheric pressure argon plasma jet

J Hnilica and V Kudrle

Department of Physical Electronics, Masaryk University, Kotlářská 2, CZ-61137, Brno, Czech Republic

E-mail: hnilica@mail.muni.cz

Received 16 October 2013, revised 16 December 2013
Accepted for publication 30 December 2013
Published 7 February 2014

Abstract

The effects of amplitude modulation (AM) on an atmospheric pressure microwave argon jet is investigated using time-resolved optical emission spectroscopy, passive acoustic diagnostic and digital camera imaging. These techniques show significant changes of the effluent plasma properties with varying AM frequency. Operation in AM mode can enhance the plasma jet length or width over continuous-wave mode with the same mean power, which could be advantageous in many practical applications of plasma jets.

Keywords: plasma jet, atmospheric pressure plasma, amplitude modulation, plasma diagnostics, optical emission spectroscopy

(Some figures may appear in colour only in the online journal)

1. Introduction

Low temperature atmospheric pressure plasma discharges are widely used in various technological applications like plasma surface modification, activation, plasma-enhanced chemical vapour deposition (PECVD) of thin films or plasma decontamination of toxic compounds [1–6]. Nowadays, there is a lot of research directed to the use of such plasma discharges in plasma medicine and biomedical applications [7–9].

Discharges excited using pulsed or modulated power are of considerable interest for many applications including materials processing. They can have higher average charged particle densities at the same average power and significantly lower thermal loading of the substrate. Both effects can be attributed to a non-linear relation between the supplied power, electron temperature and gas temperature. In addition, the negative ions in electronegative plasmas may be able to escape during the off-time, which can be useful in certain types of processing [10].

From a point of view of the fundamental plasma physics research, the pulsed discharge technique is a powerful tool for the study of the plasma kinetics. Numerous studies have been performed concerning kinetics of neutrals, excited species as well as charged particles [11–16].

Surface-wave driven discharges are often used for both research and applications as they can be easily generated in large dimensions (both 1D and 2D). Their operation in a pulsed regime was investigated, naturally, too. Most of these studies were carried out in low pressure plasmas and dealt with the ionization front velocity, the rise time of the pulse and the axial profiles of the plasma density [17–20].

This work focuses on atmospheric pressure discharge and instead of simple on-off pulsation the excitation power is continuously modulated by a sinusoidal waveform. A microwave (MW) jet operated in argon was chosen as a typical representative of atmospheric pressure surface-wave discharges.

In our previous work [21] it was found that filamentary nature [22, 23], typical for the argon jet, can be easily affected by small variations in experimental conditions. Therefore only non-invasive diagnostics such as digital imaging, time-resolved optical emission spectroscopy (OES) and passive acoustic analysis were considered so the delicate balance is not disturbed.

The radial contraction in atmospheric argon plasmas may be a problem in certain applications. Until recently it was typically solved by adding some molecular admixture. However, it seems possible [24] to achieve this by adding a small amount of different rare gas, too. The problem of radial contraction and filamentation can be also partly compensated

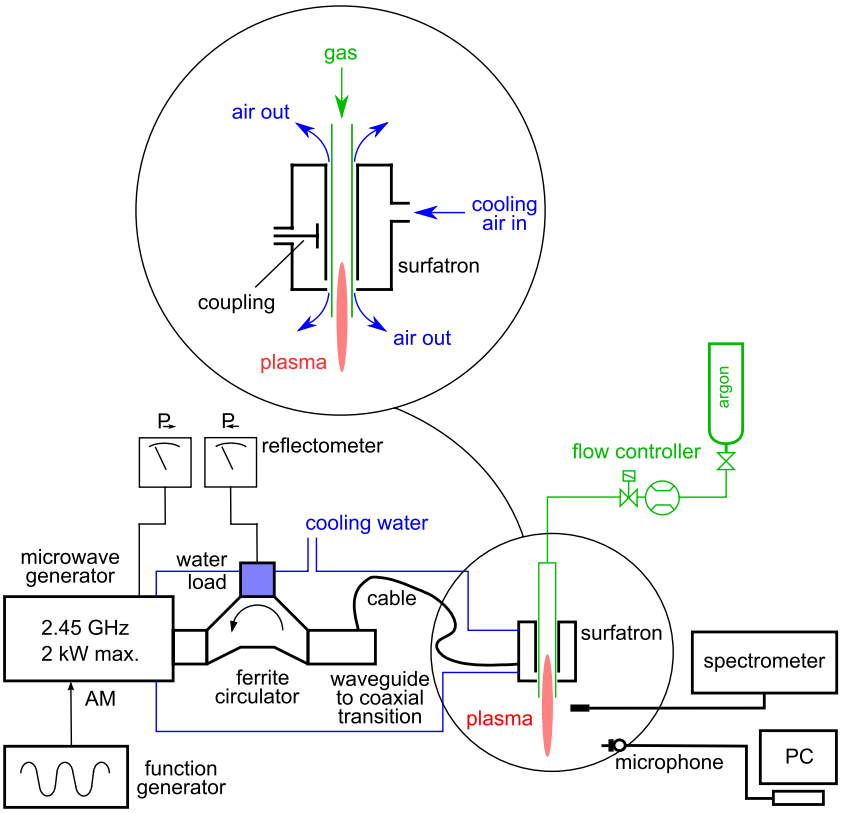

Figure 1. Schematic drawing of the experimental set-up.

by a temporally optimized de-localization of filament(s). One of the goals of the presented work is to study the possibility of influencing the plasma shape (and by consequence, its diameter) by the power modulation alone.

2. Experimental set-up and procedure

Figure 1 shows the design of the experiment. Besides the studied MW plasma source (surfatron), it is equipped with a system for optical spectroscopy, a microphone and a recording system for the emitted acoustic signals and high-speed low resolution and low-speed high resolution cameras for plasma imaging.

The surface-wave discharge was produced by applying the microwave power to a gas flowing in a narrow discharge tube. The magnetron generator SAIREM GMP 20 KED (2.45 GHz) has been operated in the amplitude modulated (AM) mode using a function generator. A sinusoidal AM envelope with 150 W minimum, 350 W maximum and 250 W mean power was used in this work. The MWs were fed from the magnetron to the surface-wave launcher—surfatron [25] (SAIREM Surfatron 80 with integrated matching)—via waveguide, ferrite circulator, reflectometer and coaxial cable. The calibrated diodes of the reflectometer gave the forward and reflected power. The matching was adjusted to maintain the reflected power below 10 W. The surfatron design consists of a coaxial resonant cavity with a narrow wave launching gap around a fused silica discharge tube (170 mm in length, 1.5 mm and 4 mm inner and outer diameter, respectively). The end of the discharge tube was 2 cm from the launching gap. The argon was flowing through the discharge tube at a rate of 1.45 slm (standard litre per minute) set by a mass flow controller.

The discharge tube is externally cooled by compressed air, whereas the generator, the circulator and the surfatron by water.

During the experiments, the ambient conditions were 23 °C temperature and 47–56% air humidity.

2.1. Optical analysis

A digital camera (Nikon D3100 with objective Nikon 55–300 mm f/4.5–5.6 G AF-S DX VR) was used for low-speed high resolution images with 2 s exposition time.

A high-speed camera (Olympus i-SPEED 2) operating in framing mode was used to study the plasma evolution in time. At 8000 frames per second its maximum resolution is 320 × 240 pixels. The zoom of the camera lens was set in such manner as to project the plasma jet over a substantial part of the sensor.

OES has been carried out using a Jobin-Yvon Horiba FHR1000 spectrometer (Czerny-Turner configuration) with 1 m focal length and 2400 grooves mm^{-1} grating. An intensified CCD camera (Andor IStar 720) at the exit port of the spectrometer served as the detector. The specified spectral resolution is 8 pm, whereas the time resolution is in order of nanoseconds. The relative spectral sensitivity of the spectrometer was calibrated using a tungsten–halogen lamp in the spectral range from 200 to 750 nm. The accuracy of line intensities is typically given mainly by the photon noise which is proportional to the square root of the number of collected

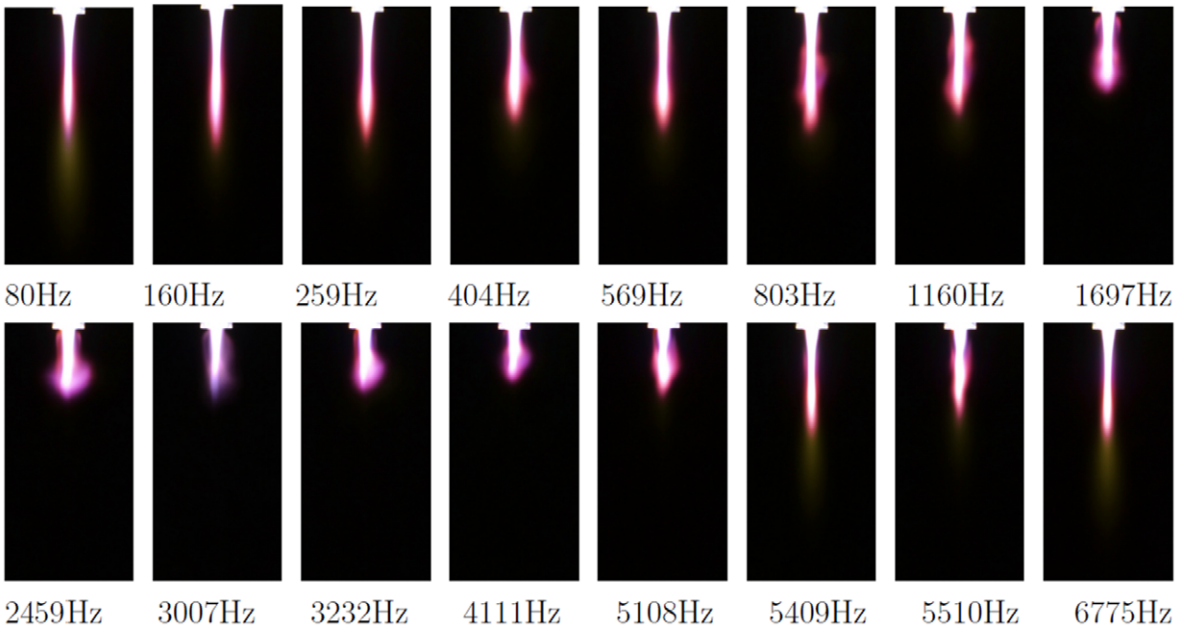

Figure 2. Influence of AM on the shape of the plasma. All measurements are carried out under same operational conditions, i.e. same mean power, same Ar flow rate, etc, except changes in the AM frequency. For a scale, the outer diameter of the discharge tube, visible at the top of the images, is 4 mm. The exposition time is 2 s.

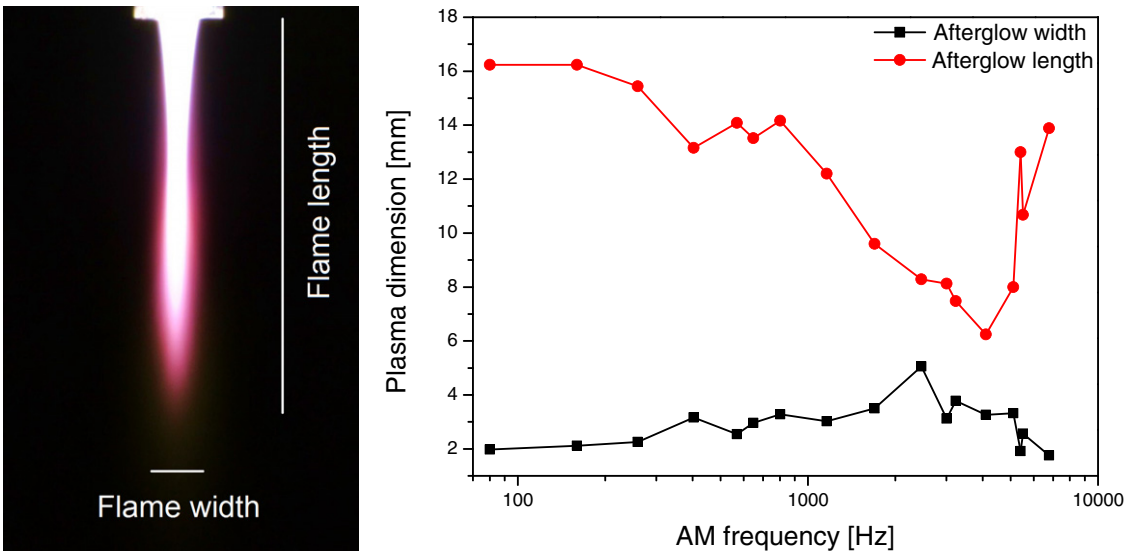

Figure 3. On the left, the definitions of the plasma flame length and flame width are shown. On the right, there is dependency of these on the AM frequency.

photons. Therefore the total integration time was set to achieve sufficient line intensities.

The optical fibre was placed 2 mm downstream from the discharge tube end and perpendicularly to the discharge axis. The fibre aperture collected the light emitted effectively from the whole diameter of the discharge. The overview spectra were recorded with integration time adjusted to achieve good data quality in the areas of Ar I lines (414–750 nm) and in the OH band (transition $A\,^2\Sigma^+ \rightarrow X\,^2\Pi$, 300–312 nm). Besides the integral measurements, the Ar I lines and OH band intensity were also studied in time-resolved manner, i.e. in synchronization with the function generator driving the AM.

2.2. Sound analysis

Passive acoustic diagnostics represent another alternative to the foregoing diagnostic methodologies as they are low cost and truly non-invasive [26, 27]. The emitted acoustic signal generated by the discharge at the tube opening was captured by using a microphone, which was mounted 10 mm downstream of the plasma tube end and 85 mm off the plasma axis to avoid disturbing the gas flow and plasma itself. The signal from the microphone was recorded continuously at 16 bit resolution with sampling rate of 44100 Hz by built-in computer sound card. The frequency sensitivity of the microphone was not calibrated but as it was ordinary microphone for voice

recording, its sensitivity in the 10^2–10^4 Hz range was sufficient for the present study.

To study the response of the plasma at different modulation frequencies, a chirp modulating signal was digitally synthesized. During its 300 s duration, its frequency logarithmically increased by 1 decade per 100 s, going from 10 Hz at 0 s to 10 kHz at 300 s. The amplitude and offset of this signal was then adjusted to get the MW power in the range 150 W–350 W with 250 W mean.

The sound analysis was carried out using Matlab compatible GNU Octave software [28, 29]—mainly its `specgram()` function. After windowing (500 ms Hann function) and Fourier transformation, it produced power spectral density in 250 ms long spectral slices.

3. Results and discussion

All the measurements are carried out under same operational conditions, i.e. same mean power, same Ar flow rate, etc, except the changes in AM frequency.

3.1. Low speed high resolution photographs

The atmospheric surface-wave plasma appears in a typical elongated columnar form, starting in the discharge tube and ending in flame-like diffuse plume outside the discharge tube itself. The low frequency (10–10000 Hz) AM modulation has a profound effect (see figure 2) on discharge plasma, probably due to interaction between AM frequency and acoustic eigenfrequencies of the system itself, see section 3.5. The digital imaging (see figure 2) reveals the changes of the effluent plasma shape and a presence or absence of the visual emissions from the yellow afterglow (caused by atomic nitrogen reassociation [30, 31]) depending on the AM frequency. The latter means that the plasma chemistry is affected, too. In AM frequency range 803–5108 Hz and at 5510 Hz, a 'halo' effect is observed which is caused by transient microfilaments perpendicular to the primary plasma channel. Their position being random, at long exposure images of figure 2 one observes only a integral halo of them. In that case the visible plume diameter is approximately two times wider than for other frequencies, when a halo effect is not observed. Such broadening could be interesting for applications as the width of the plume can be controlled simply by the AM frequency.

The lengths of the flame and flame width were estimated from the images by pixel analysis and they are shown in figure 3. In the range 80–803 Hz the flame length is changing only slightly. But for higher frequencies (1000–4000 Hz) the flame becomes shorter until a minimum is reached at 4111 Hz AM. This is also the turning point and the flame starts to get longer. For the flame width the trend is reversed. A maximum (5.1 mm) is reached at 2459 Hz, which means that the plasma is more than three times wider than the inner diameter of the discharge tube.

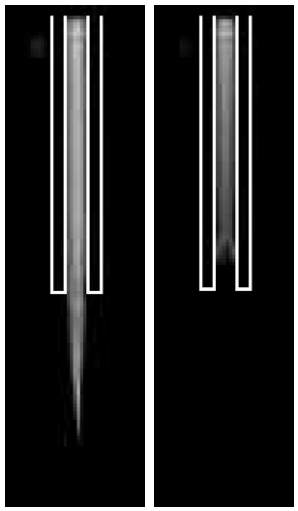

Figure 4. Typical images of the change of the plasma length due to AM of the input power. On the left there is the discharge at the highest point of the AM envelope and on the right there is at the lowest point of the AM envelope. Modulation frequency is 80 Hz and exposition time is 1/8000 s.

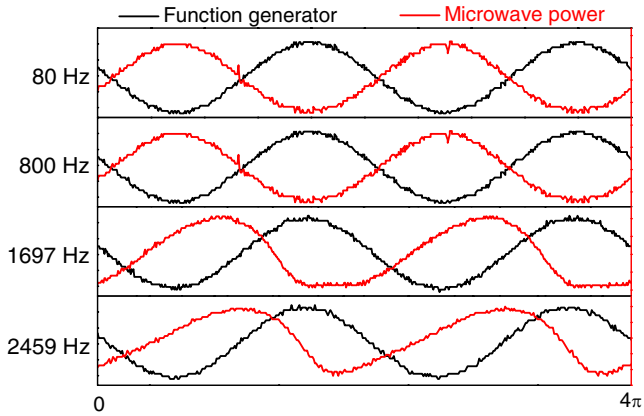

Figure 5. Comparison of signals from the function generator and the MW generator for four selected frequencies.

3.2. High speed low resolution photographs

Figure 4 demonstrates the changes of discharge length during the amplitude modulation (AM). On the left, there is the discharge at the highest point of the AM envelope. On the right, the discharge is shortened at the lowest point of the AM envelope. There is experimental evidence that temperature (from OH spectra) changes, too (see figure 11). As the plasma gas is cooling down, the local pressure decreases and the gas flow is affected. The effective gas velocity could decrease or it could be even negative. It implies that the surrounding air could be sucked in. During the experiments with AM, the intensive acoustic emissions from the plasma were observed for certain drive frequencies (more details are in section 3.5). It means that the local change of the pressure really takes place.

3.3. Selected AM frequencies and corresponding distortion

Four AM frequencies (80, 800, 1697 and 2459 Hz) from figure 2 were chosen as the representatives for subsequent

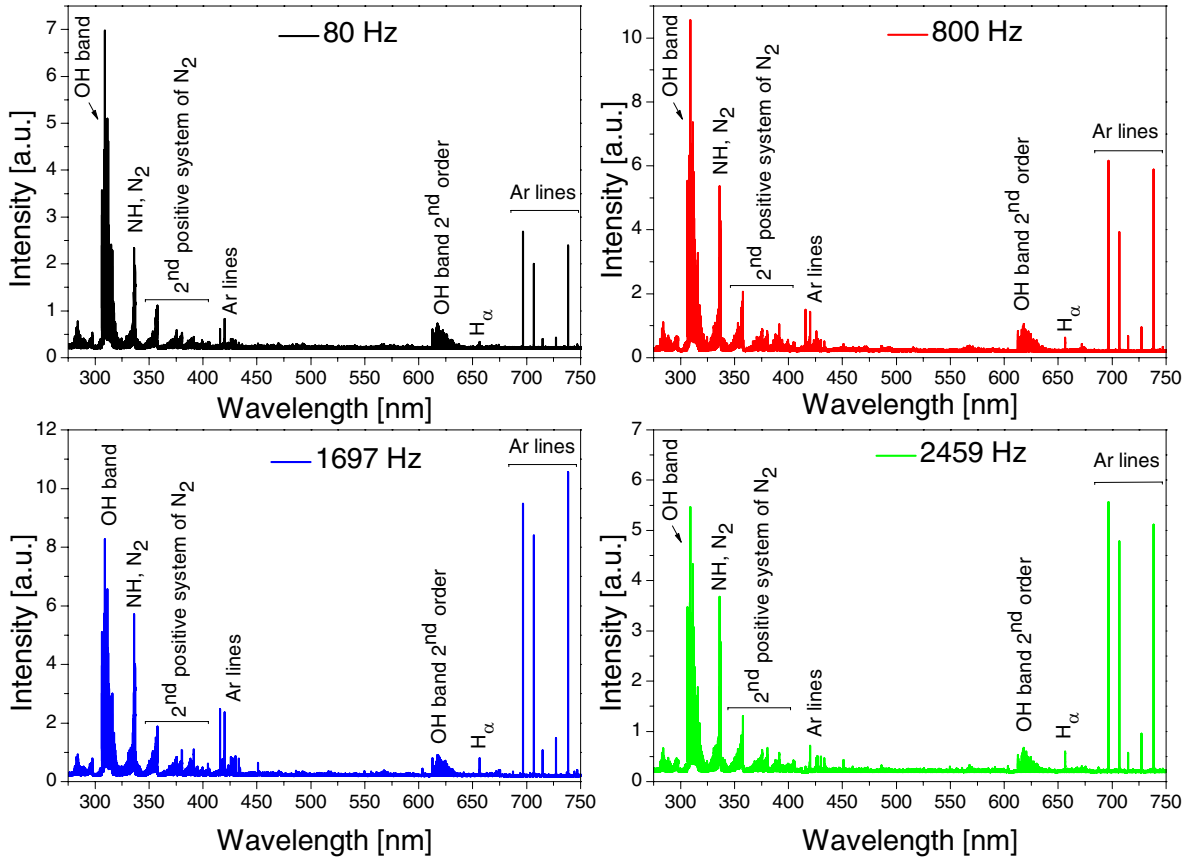

Figure 6. Overview emission spectra of the effluent plasma (outside the discharge tube) for four AM frequencies, other experimental parameters being the same. In this figure the spectra were not corrected by the spectral sensitivity of the spectrometer.

studies. The frequency 80 Hz was chosen because the plasma has typical narrow columnar shape. At 800 Hz we can observe for the first time the halo effect. At 1697 Hz AM the discharge is getting shorter and produces strong acoustic emissions. The plasma shape at 2459 Hz is typical for several successive frequencies in figure 2 and 3, the plasma is the widest and the acoustic emission is the strongest, too. Consequently, they include both low and high frequencies as well as four different effluent flame shapes, too.

The signal from MW generator was tested for possible distortions. In figure 5 there are shown the signals from the forward power detector and from the function generator driving the MW generator. To normalize the time scale for different AM frequencies, the phase ($\omega \cdot t$) is used on the horizontal axis. For 80 and 800 Hz there is no observable distortion or shift of the signal. One can see a slight distortion and time shift for the 1697 and 2469 Hz frequencies, as the response of the modulator circuit is not instantaneous.

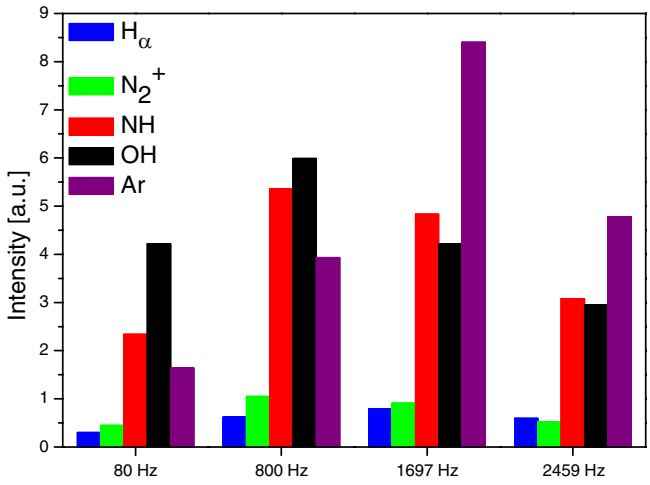

Figure 7. Intensities of selected lines and bands in the overview spectra (figure 6) for selected modulation frequencies.

3.4. OES measurements

3.4.1. Overview spectra. The time-integrated overview optical emission spectra, recorded in the range 275–750 nm, are shown in figure 6. The measurement zone is outside the discharge tube (i.e. in the open atmosphere, 2 mm downstream from the discharge tube end) and so besides argon also other spectral features are present due to a mixing with surrounding air.

It can be seen that the most intensive spectral lines belong to Ar I lines (700–750 nm), OH system ($A\,^2\Sigma^+ \rightarrow X\,^2\Pi$, 306–312 nm) and N_2 ($C\,^3\Pi_u \rightarrow B\,^3\Pi_g$) bands—the vibrational transitions 0–0 (bandhead at 337.1 nm) and 0–1 (357.7 nm), and to NH band (336 nm). The H_α line (656 nm) and a weak second order of OH system (610–630 nm) are also distinguishable.

It should be noted that OES cannot fully determine the composition of the plasma as some species can be in the ground

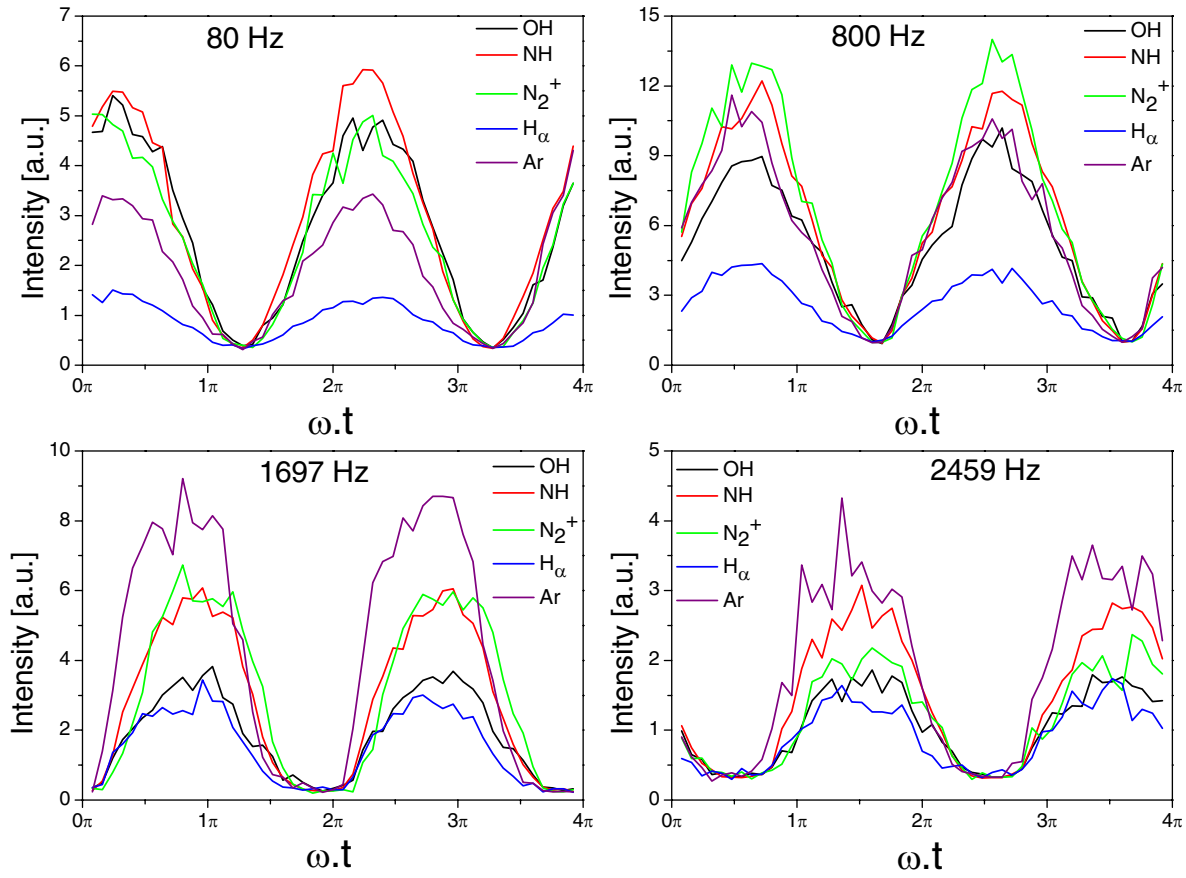

Figure 8. Time-resolved evolution of the selected spectral lines emitted from effluent plasma for four AM frequencies.

state or their emission lines (or bands) are outside the observed wavelength range. E.g. the ozone, despite being produced by the jet [32], is not observed in our emission spectra.

In figure 7 the intensities of the most prominent spectral features are plotted for different modulation frequencies. It reveals that with increasing modulation frequency the intensities of all selected lines and bands follow a similar trend—they increase at first, then reach a maximum and finally fall again. However, the position of the maximum is not the same for all the species. Argon and hydrogen reach the maximum at 1697 Hz, whereas the NH, N_2^+ and OH reach the maximum sooner, at 800 Hz. The discriminating factor between these two groups seems to be the excitation energy, as Ar and H lines need >11 eV, while NH, N_2^+ and OH band need <6 eV [33–35]. The shift in the maxima then probably reflects the shape of electron energy distribution function (EEDF).

3.4.2. Time-resolved evolution of the selected lines. In the previous section the most significant lines and bands in time-integrated overview optical emission spectra were discussed. In the following, the selected lines are investigated in more detail in a time-resolved manner for the chosen AM frequencies. As the representative lines were chosen: Q_1 (13/2) line at 308.73 nm from OH band, NH line at 336.00 nm, N_2^+ at 391.40 nm, H_α at 656.27 nm and Ar I line at 706.72 nm. Figure 8 shows the temporal evolution of the areas under these lines. Again, to normalize the time scale for different AM frequencies, the phase ($\omega \cdot t$) is used on the horizontal axis. For 80 and 800 Hz all lines follow the sinusoidal AM envelope very well. Nevertheless, for 1697 Hz and in particular for 2459 Hz the argon intensity shows significant deviation from sinusoidal to a more trapezoidal shape.

3.4.3. Excitation temperature estimated from Ar I lines. Electron temperature (T_e) is one of the most important plasma parameters, as it directly influences nearly all ionization and excitation processes. For plasmas in partial local thermodynamic equilibrium (pLTE), the population of top atomic levels obeys the Saha equation which also implies a Boltzmann balance at equilibrium [36]. Therefore, the excitation temperature (T_{exc}) derived from the Boltzmann plot is often considered equal to the electron temperature [33, 37, 38].

From the time-resolved and multiply accumulated intensities of the selected lines (this particular selection have been used also by other investigators [34, 37, 39]) the relevant temperatures using a simple Boltzmann plot technique [40] was calculated, see figure 9. The excitation temperature calculated from these Ar I emission lines is for 80 Hz in the range (3400–4100) K and it follows the sinusoidal AM envelope very well. During the whole AM period the statistical errors are roughly the same (4%), i.e. ±150 K. For 800 Hz the temperature is going from (3600±150) K to the (4500±500) K in the maximum of the AM envelope. Despite the growth of the

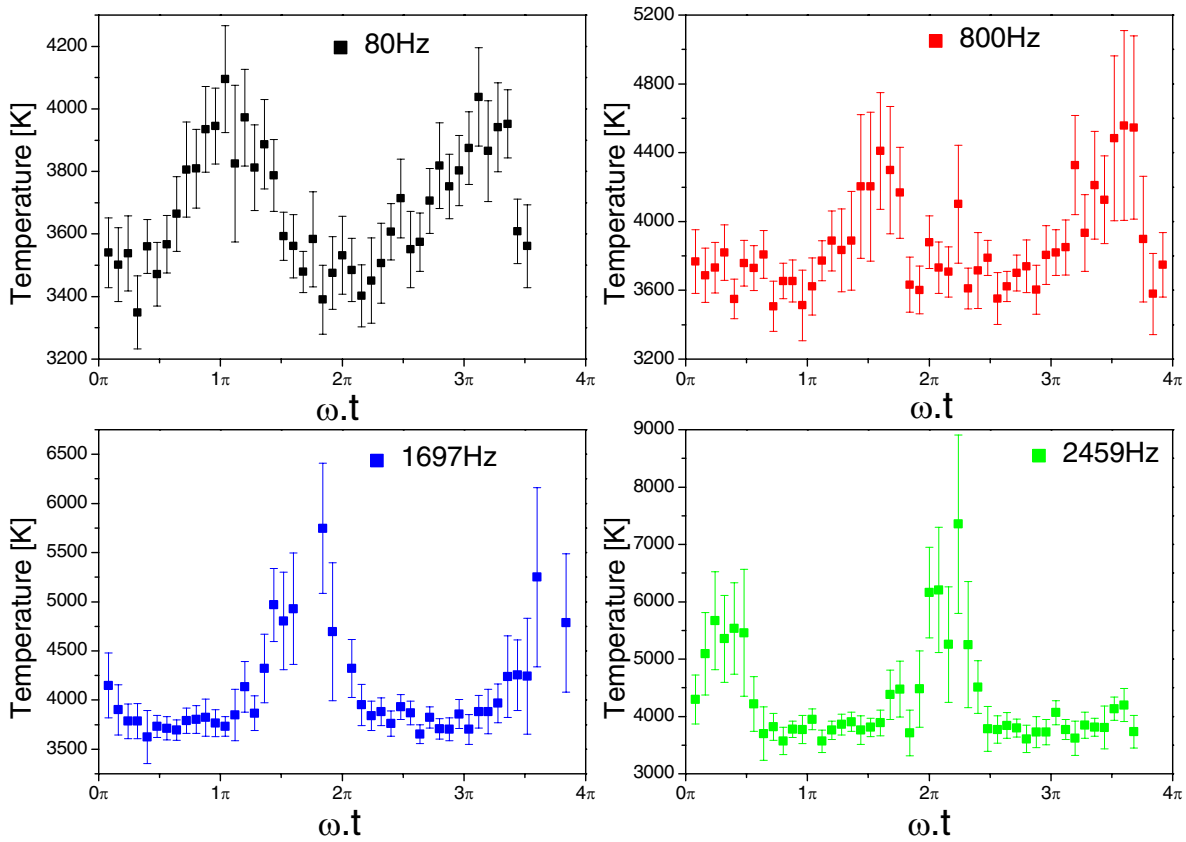

Figure 9. Time-resolved plasma excitation temperature calculated from Ar I lines.

temperature error from 4% to 11% the excitation temperature still follows the sinusoidal shape. Nevertheless, the increase and decrease of the temperature does not take exactly half of the period as it has for 80 Hz AM. The statistical error in the temperature maximum is two times higher than that for the rest of the period.

For other two frequencies (1697 and 2459 Hz) the graphs of the excitation temperature do not strictly follow sinusoidal behaviour. T_{exc} is for a greater part of the period rather constant and rapidly increases and decreases just at the maximum, which is 5750 K and 7500 K for 1697 Hz and 2459 Hz, respectively. The temperature error is much higher (20%) at the maximum than for the rest of the period, where the temperature statistical error is around 5%.

This changes in statistical error lead to the conclusion that Boltzmann statistics is valid for 80 and 800 Hz during the whole AM period, whereas for 1697 and 2459 Hz it is valid only for a part of the sinusoidal AM envelope.

The figure 10 shows the Boltzmann plots for four distinct experimental conditions, i.e. for 80 and 1697 Hz AM, each in both minimum and maximum of AM.

It is clear that for 80 Hz AM, both in minimum and maximum, and for 1697 Hz in the AM minimum the position of experimental points near the straight lines in the graphs validate the assumption of Boltzmann statistics. In contrast, for the maximum of 1697 Hz AM, the graph (bottom right) indicates that Boltzmann statistics is not valid.

It is interesting to note that maxima of the temperature in figure 9 are not exactly synchronous with maxima of the intensities in figure 8. This suggests certain complexity of the excitation and energy transfer processes involved. The average excitation temperatures for all AM frequencies are consistent with measurements made on the same plasma device by [32].

The excitation temperature was also calculated for CW input power. T_{exc} is (2703 ± 82) K which is about 700 K lower temperature compared to the mean excitation temperature for 80 Hz AM.

3.4.4. Rotational temperature estimated from OH($A-X$) band. The intensities of molecular bands could be used to infer the rotational temperature from the Boltzmann distribution function. Usually, the rotational temperature is an excellent indicator of the gas temperature due to the balance between the rotational and translational degrees of freedom established in plasmas at atmospheric pressure [35, 41, 42].

The molecular emission bands of OH transitions were used to determine the rotational temperatures as the OH molecular bands were intense and easily observed in all experimental conditions. This chemical species has often been applied as a 'thermometer tool' in high pressure systems [7, 37, 43–47] (the relaxation of rotational states is much faster than the electronic transitions). The Boltzmann plot technique is for OH quite straightforward, as continuum background is rather small and no spectral calibration of the optical system is needed as lines are close in wavelengths. However, one should be always aware of potential difficulties associated with self-absorption, non-Boltzmann rotational population distribution and interferences with other species present in the plasma [48].

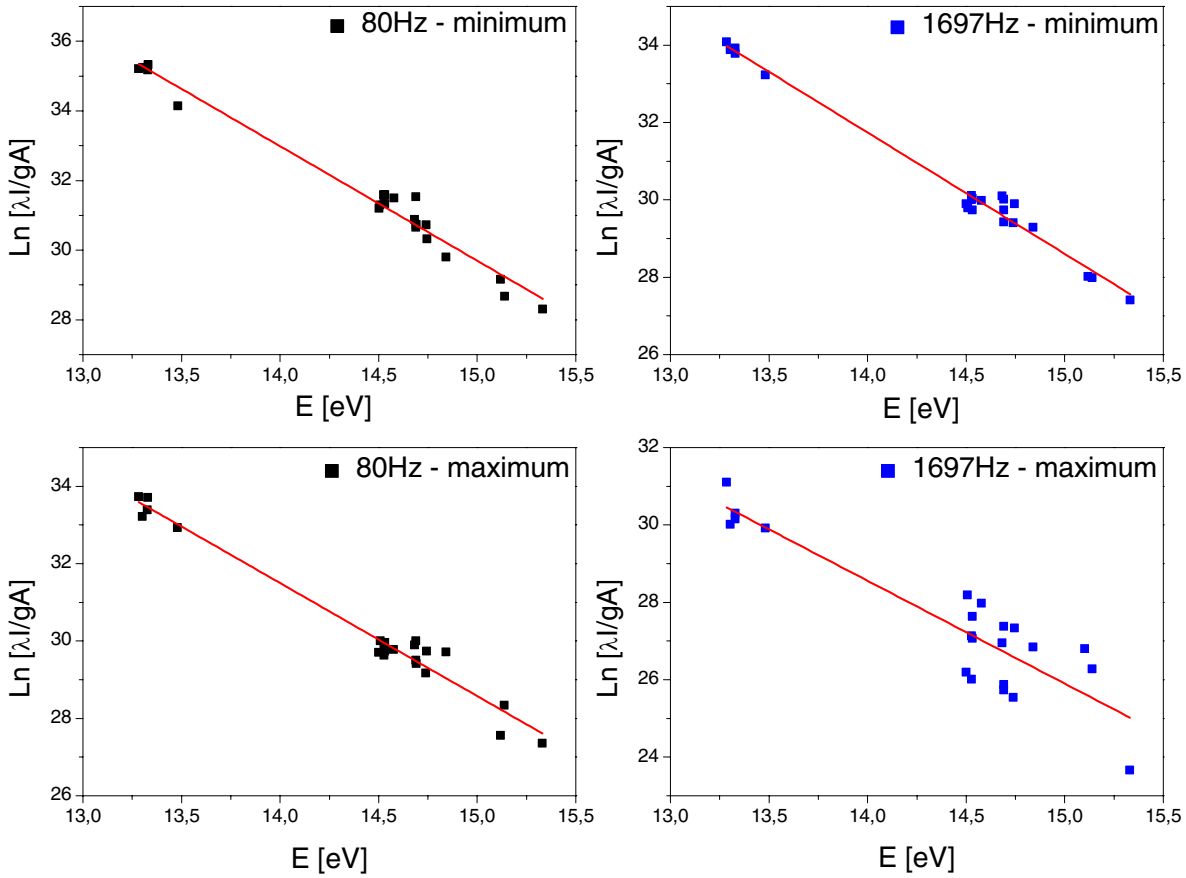

Figure 10. The selected Boltzmann plots used for calculation of excitation temperature in figure 9. The graphs are shown for (top left) 80 Hz and $\omega t = 1.84\pi$, (top right) 1697 Hz and $\omega t = 2.8\pi$, (bottom left) 80 Hz and $\omega t = 1.2\pi$, and (bottom right) 1697 Hz and $\omega t = 1.84\pi$.

Table 1. List of the OH spectral lines together with their parameters used for determining the rotational temperature using a Boltzmann plot.

Line	λ (nm)	E (cm^{-1})	A (10^8 s^{-1})
$Q_1(9/2)$	308.3278	32.779	33.7
$Q_1(11/2)$	308.5196	32.948	42.2
$Q_1(13/2)$	308.7338	33.150	50.6
$Q_1(17/2)$	309.2394	33.652	67.5
$Q_1(19/2)$	309.5324	33.952	75.8
$Q_1(21/2)$	309.8586	34.283	84.1

In this paper the Boltzmann plot technique implemented in Spectrum Analyzer software [49] was used to determine the rotational temperature using the intensities of certain OH lines (table 1). This particular selection of lines was used also by other authors [37, 50, 51].

The time-resolved rotational temperature (figure 11) calculated from the rotational-vibrational OH band oscillates synchronously with the power envelope between 1600 and 2150 K with 15% statistical error. However, its shape deviates from the purely sinusoidal 80 Hz AM as the increasing part is two times longer than the decreasing part.

For 800 Hz AM the temperature varies between 1650 and 2400 K, but the statistical error in the maximum is much higher (25%). Also for this frequency the increase in the temperature takes two times longer than the decrease and so the sinusoidal shape is almost unrecognizable.

For higher modulation frequencies, the temperature of gas is not able to follow the rapidly varying incident power and it is approximately 2500 K for 1697 Hz AM and 2000 K for 2459 Hz AM, respectively. This effect has the same principal cause as the non-equilibrium itself—slow energy cascade from the electronic excitations to translational ones.

The temperature error is much higher (>30%) in the maximum than for the rest of the period, where the temperature error is for all studied frequencies around 15%. Corresponding Boltzmann plots are in figure 12. Rotational Boltzmann statistics is valid for 80 Hz during the whole period. But for 800, 1697 and 2459 Hz it is valid just for the lower parts of the temperature curve. For these frequencies then the rotational levels of the OH(A) state do not always follow a Boltzmann distribution, so it is not possible to directly infer the translational temperature of the gas from the OH(A–X) band measurement. At the maximum, the discharge is probably in a strongly non-equilibrium state.

However, at the first sight this is not to be expected at atmospheric pressure where the collisional time is significantly shorter than the radiative life time of OH(A) (which is of order of 700 ns) and multiple collisions can occur before the excited OH(A) state radiates. Departure from a rotational Boltzmann distribution may occur, e.g. as a result of preferential quenching of the rotational levels of OH [41]. The discussion of non-Boltzmann behaviour and its consequences for the

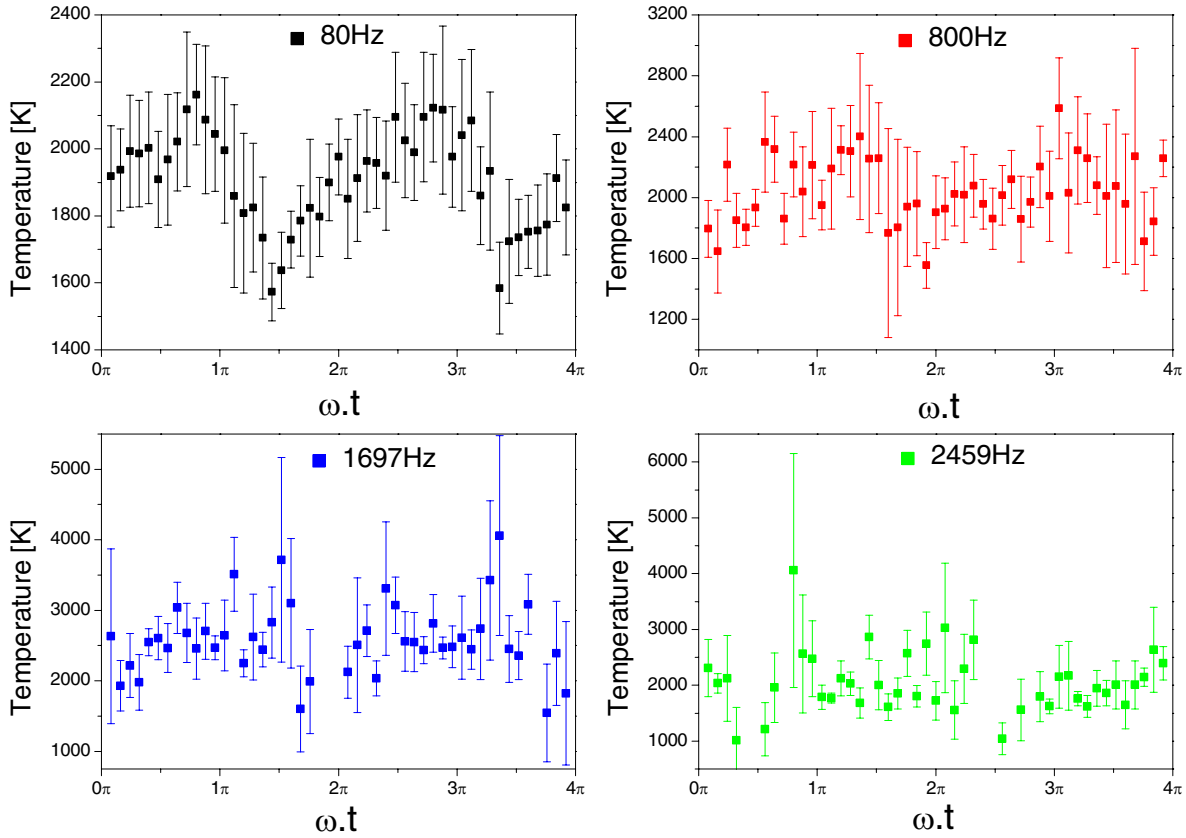

Figure 11. Time-resolved rotational temperature calculated from OH system for four AM frequencies.

interpretation of the temperature can be found in, e.g., [41, 52, 53].

For CW mode the T_{rot} is (2043±217) K which corresponds to the mean rotational temperature for 80, 800 and 2459 Hz of the AM.

3.5. Sound analysis

When working with different modulation frequencies we observed that for certain AM frequencies a strong acoustic signal was produced by the plasma as was mentioned in section 3.4.1. Therefore the process was investigated in more detail. A logarithmic chirp signal was digitally synthesized, starting at 10 Hz and increasing to 10 kHz during 300 s, as an input for MW power modulation. The mean power, as well as minimum and maximum value, remained the same as in other experiments in this paper. In the same time, the sound emitted by the plasma was continuously recorded. This record then contains the frequency dependence of audio response of the plasma to varying AM frequency. The recorded signal was windowed and processed by fast Fourier transform (FFT) into the form of time dependent power spectral density, shown in figure 13.

In this graph, the x-axis corresponds to elapsed time. On y-axis, there is frequency. The colour shows the intensity of the response, where the blue colour corresponds to low intensity and the red to high intensity. We can observe several notable things. There is curved line going from 10 Hz at $t = 0$ s to 10 kHz at $t = 300$ s. This is the 'driving' signal, i.e. the logarithmic chirp mentioned above. This is expected, as the periodic changes in MW power cause periodic changes of gas temperature and consequently to local pressure changes. Sound waves with the same frequency as the envelope of AM modulated MWs are thus produced. The line is curved because logarithmic and not linear chirp was used. Besides this fundamental frequency response, several higher harmonic frequencies with an intensity decreasing with the order of harmonics are visible. One can observe also some diffuse horizontal stripes, most clearly in the left and centre part of the figure. This audio signal does not depend on AM modulation which means that it has different cause. The striping suggests that it is not white noise, but that certain frequencies are more emphasized. These most probably correspond to eigenfrequencies of the system consisting of fused silica discharge tube filled by argon gas with strong temperature gradients in the gas. The interesting things happen when the driving signal frequency coincides with one of these eigenfrequencies of the system. First occurrence of this phenomenon in figure 13 happens at $t = 228$ s. Unexpectedly, the response of the system is not harmonic, but broadband. This exhibits itself as vertical stripe covering nearly the full range of observed frequencies. As the chirp signal slowly increases the AM frequency, the drive and eigenfrequencies drop out of 'resonance' and audio emissions become quiet again. Later, at another intersection of drive and eigenfrequency ($t = 240$ s) the situation repeats again. For driving frequencies higher than approx. 7 kHz no

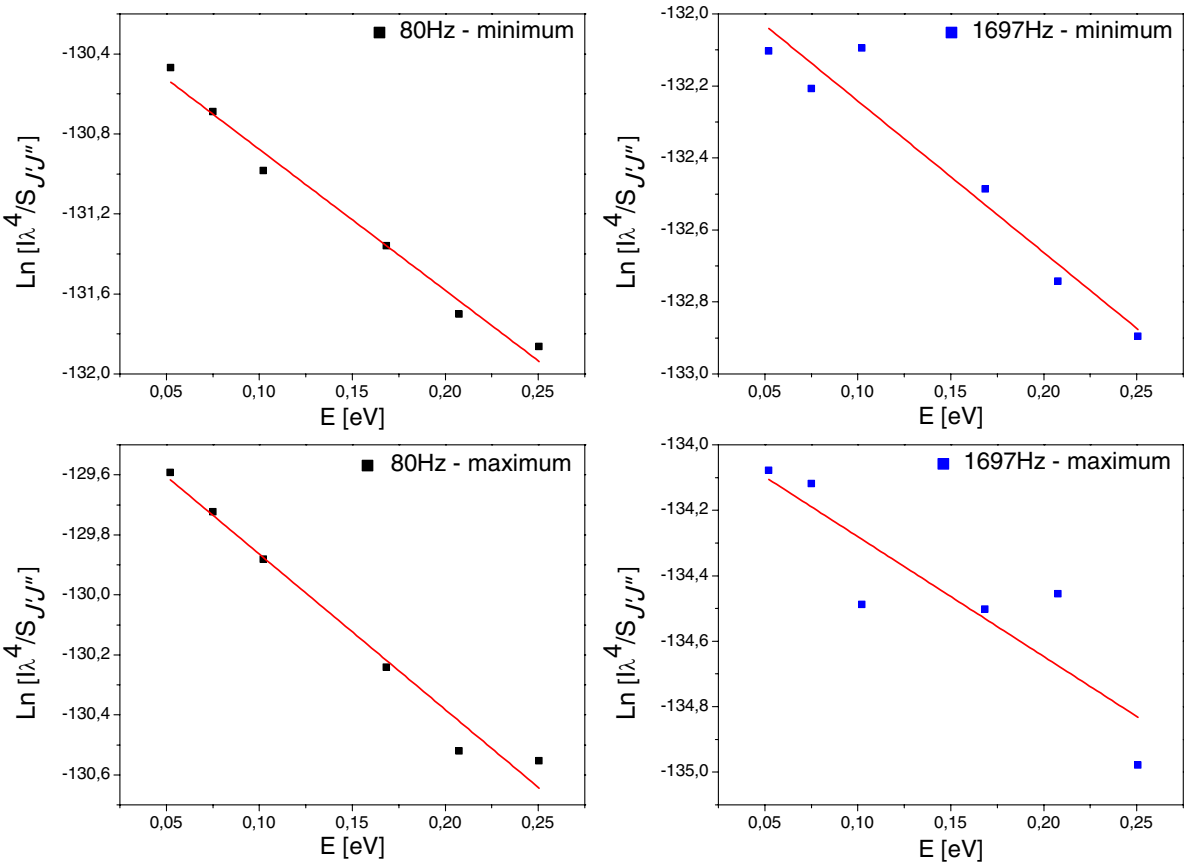

Figure 12. The selected Boltzmann plots used for calculation of rotational temperature in figure 11. The graphs are shown for (top left) 80 Hz and $\omega t = 1.52\pi$, (top right) 1697 Hz and $\omega t = 0.72\pi$, (bottom left) 80 Hz and $\omega t = 0.8\pi$, and (bottom right) 1697 Hz and $\omega t = 1.60\pi$.

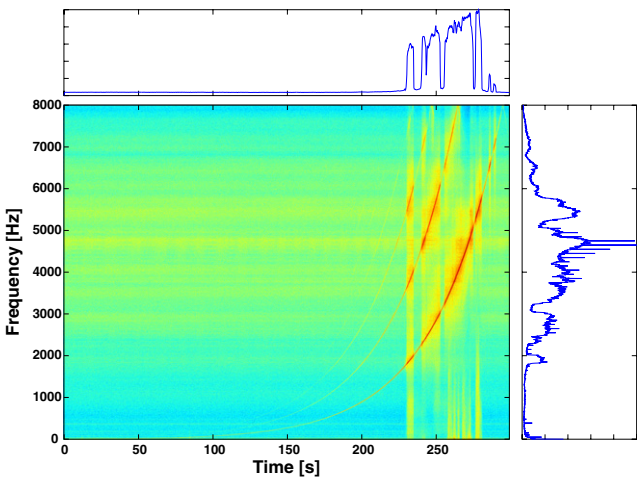

Figure 13. Frequency response of the MW atmospheric jet to AM modulation by logarithmic chirp signal.

'resonances' were observed, probably due to the limitations of the modulator.

In the same figure, there are two other sub-plots. The top one corresponds to total magnitude of the sound (all frequencies) as it depends on time, and by consequence on driving signal. As the driving frequency of AM increases, the system goes through several intervals of loudness and quietness. The intervals of strong acoustic emissions are directly related to broadband noise appearing at 'resonances'. The right sub-plot shows the time-averaged spectrogram. The horizontal diffuse bands in main figure are reflected as broad maxima in this graph.

The analysis of figure 13 provides direct proof of existence of strong pressure waves in AM modulated discharge, which explains the changes in discharge appearance discussed in section 3.1. The acoustic pressure waves influence the flow of working gas and can even promote a back-propagation of the air into the discharge tube. This is naturally reflected by changes in the plasma appearance. The incoherent nature of the response in 'resonances' is the evidence that the processes involved in coupling between the input power, gas temperature and gas flow are non-linear and stochastic. The non-sinusoidal and stochastic response of rotational temperature (see figure 11 in section 3.4.4) for drive frequencies 1697 and 2459 Hz is then not surprising.

4. Conclusions

The sinusoidal power modulation of a microwave plasma jet strongly and non-linearly affects the processes in the plasma. This is emphasized by the fact that in a plasma jet expanding to surrounding air, the periodic changes in local temperature and pressure influence the back-diffusion of air into the working gas. Digital imaging shows changing shape and colour of the

effluent plasma, depending on the modulation frequency. This is accompanied by changes in excitation and gas temperatures. However, in certain conditions, the plasma is not in thermal equilibrium and so the determination of temperature has rather high statistical error. The periodic modulation-induced pressure oscillations exhibit themselves as strong acoustic signal. The analysis of these sound emissions for varying modulation frequencies reveal certain resonances between eigenfrequencies of the system and the AM driving frequency. The ability of controlling the shape and the properties of the plasma jet by the modulation frequency, mean power being constant, open a new, simple, possibility of optimizing the plasma jet for certain applications.

Acknowledgments

This research has been supported by the project R&D center for low-cost plasma and nanotechnology surface modifications CZ.1.05/2.1.00/03.0086 funded by European Regional Development Fund. Authors are thankful to V. Aubrecht for lending the high-speed camera.

References

[1] Kogelschatz U 2003 *Plasma Chem. Plasma Process.* **23** 1
[2] Wagner H E, Brandenburg R, Kozlov K V, Sonnenfeld A, Michel P and Behnke J F 2003 *Vacuum* **71** 417–36
[3] Shenton M J, and Stevens G C 2001 *J. Phys. D: Appl. Phys.* **34** 2761
[4] Trunec D, Zajickova L, Bursikova V, Studnicka F, Stahel P, Prysiazhnyi V, Perina V, Houdkova J, Navratil Z and Franta D 2010 *J. Phys. D: Appl. Phys.* **43** 225403
[5] Schäfer J, Foest R, Quade A, Ohl A and Weltmann K D 2008 *J. Phys. D: Appl. Phys.* **41** 194010
[6] Herrmann W, Henins I, Park J and Selwyn G S 1999 *Phys. Plasmas* **6** 2284
[7] Stoffels E, Flikweert A J, Stoffels W W and Kroesen G M W 2002 *Plasma Sources Sci. Technol.* **11** 383–8
[8] Lee J K, Kim M S, Byun J H, Kim K T, Kim G C and Park G Y 2011 *Japan. J. Appl. Phys.* **50** 08JF01
[9] Weltmann K D, Polak M, Masur K, von Woedtke T, Winter J and Reuter S 2012 *Contrib. Plasma Phys.* **52** 644–54
[10] Lieberman M A and Lichtenberg A J 2005 *Principles of Plasma Discharges and Materials Processing* (New York: Wiley)
[11] Wouters M J, Khachan J, Falconer I S and James B W 1998 *J. Phys D: Appl. Phys.* **31** 2004–12
[12] Behle S, Brockhaus A and Engemann J 2000 *Plasma Sources Sci. Technol.* **9** 57–67
[13] Rousseau A, Teboul E and Sadeghi N 2004 *Plasma Sources Sci. Technol.* **13** 166–76
[14] Britun N, Godfroid T, Konstantinidis S and Snyders R 2011 *Appl. Phys. Lett.* **98** 141502
[15] Welzel S, Guaitella O, Lazzaroni C, Pintassilgo C D, Rousseau A and Ropcke J 2011 *Plasma Sources Sci. Technol.* **20** 015020
[16] van der Horst R M, Verreycken T, van Veldhuizen E M and Bruggeman P 2012 *J. Phys. D: Appl. Phys.* **45** 345201
[17] Gamero A, Sola A, Cotrino J and Colomer V 1989 *J. Appl. Phys.* **65** 2199–204
[18] Grozev D, Kirov K and Shivarova A 1998 *J. Phys. IV* **8** 307–16
[19] Rousseau V, Boisse-Laporte C, Leprince P and Marec J 1994 *J. Appl. Phys.* **75** 1846–8
[20] Schlüter H and Shivarova A 2007 *Phys. Rep.* **443** 121–255
[21] Hnilica J, Kudrle V, Vasina P, Schäfer J and Aubrecht V 2012 *J. Phys. D: Appl. Phys.* **45** 055201
[22] Castanos-Martinez E, Kabouzi Y, Makasheva K and Moisan M 2004 *Phys. Rev.* E **70** 066405
[23] Kabouzi Y, Moisan M, Rostaing J C, Trassy C, Guerin D, Keroack D and Zakrzewski Z 2003 *J. Appl. Phys* **93** 9483
[24] Castanos-Martinez E, Moisan M and Kabouzi Y 2009 *J. Phys. D: Appl. Phys.* **42** 012003
[25] Moisan M, Beaudry C and Leprince P 1974 *Phys. Lett.* **50** 125
[26] Tynan J, Daniels V J, Ward P, Hynes A M, Cullen J, Byrne G, Daniels S and Dowling D P 2010 *Plasma Sources Sci. Technol.* **19** 015015
[27] O'Connor N and Daniels S 2011 *J. Appl. Phys.* **110** 013308
[28] *GNU Octave* www.gnu.org/software/octave/
[29] Eaton J W, Bateman D and Hauberg S 2008 *GNU Octave Manual* Version 3 (Network Theory Limited) ISBN 0-9546120-6-X
[30] Vašina P, Kudrle V, Tálský A, Botoš P, Mrázková M, and Meško M 2004 *Plasma Sources Sci. Technol.* **13** 668–74
[31] Mrázková M, Vašina P, Kudrle V, Tálský A, Pintassilgo C D and Guerra V 2009 *J. Phys. D: Appl. Phys.* **42** 075202
[32] Wattieaux G, Yousfi M and Merbahi N 2013 *Spectrochim. Acta* B **89** 66–76
[33] Sainz A, Margot J, Garcia M C and Calzada M D 2005 *J. Appl. Phys.* **97** 113305
[34] National Institute of Standards and Technology NIST Atomic Spectra Database [Database] [On-Line] [access 1. 5. 2013] www.nist.gov/pml/data/asd.cfm
[35] Capitelli M, Ferreira C M, Gordiets B F and Osipov A I 2000 *Plasma Kinetics in Atmospheric Gases* (Berlin: Springer)
[36] Kruger C H, Owano T, Gordon M and Laux C 1992 *Pure Appl. Chem* **64** 607–13
[37] Calzada M D, Moisan M, Gamero A and Sola A 1996 *J. Appl. Phys.* **80** 46
[38] Van der Mullen J A M 1990 *Phys. Rep.* **191** 109
[39] Calzada M D, Garcia M, Luque J M and Santiago I 2002 *J. Appl. Phys.* **92** 2269–75
[40] Griem H R 1964 *Plasma Spectroscopy* (New York: McGraw-Hill)
[41] Bruggeman P, Schram D C, Gonzalez M A, Rego R, Kong M G and Leys C 2009 *Plasma Sources Sci. Technol.* **18** 025017
[42] Leblond J, Collier F, Hoffbeck F and Cottin P 1981 *J. Chem. Phys.* **74** 6242
[43] Kapicka V, Klima M, Vaculik R, Brablec A and Slavicek P 1998 *Czech. J. Phys.* **48** 1161–6
[44] Brablec A, Kapicka V, Ondracek Z, Slavicek P, Strecha M, Stastny F and Vaculik R 1999 *Czech. J. Phys.* **49** 329
[45] Foest R, Schmidt M and Becker K 2006 *Int. J. Mass Spectrom.* **248** 87
[46] Hong Y C and Uhm H S 2006 *Appl. Phys. Lett.* **89** 221504
[47] Mariotti D, Shimizu Y, Sasaki T and Koshizaki N 2007 *J. Appl. Phys.* **101** 013307
[48] Motret O, Hibert C, Pellerin S, Pouvesle J M 2000 *J. Phys. D: Appl. Phys.* **33** 1493–98
[49] Navratil Z, Trunec D, Smid R and Lazar L 2006 *Czech. J. Phys.* **56** B944–51
[50] Munoz J, Dimitrijevic M S, Yubero C and Calzada M D 2009 *Spectrochim. Acta* B **64** 167–72
[51] Gavare Z, Svagere A, Zinge M, Revalde G and Fyodorov V 2012 *J. Quant. Spectrosc. Radiat. Transfer* **113** 1676–82
[52] Bruggeman P, Schram D C, Kong M G and Leys C 2009 *Plasma Processes Polymers* **6** 751–62
[53] Bruggeman P and Leys C 2009 *J. Phys. D: Appl. Phys.* **42** 053001